Quarkonia in the deconfined phase: Effective potentials and lattice correlators

W. M. Alberico,[1] A. Beraudo,[1,2] A. De Pace,[1] and A. Molinari[1]

[1]*Dipartimento di Fisica, Teorica dell'Università di Torino and Istituto Nazionale di Fisica Nucleare, Sezione di Torino, via P. Giuria 1, I-10125 Torino, Italy*

[2]*SPhT, CEA-Saclay, 91191 Gif-sur-Yvette, France*

(Received 6 December 2006; published 13 April 2007)

The Schrödinger equation for the charmonium and bottomonium states at finite temperature is solved by employing an effective temperature-dependent potential given by a linear combination of the color-singlet free and internal energies obtained on the lattice from the Polyakov loop correlation functions. The melting temperatures and other properties of the quarkonium states are evaluated. The consistency of the potential model approach with the available lattice data on the quarkonium temporal correlators and spectral functions is explored.

DOI: 10.1103/PhysRevD.75.074009 PACS numbers: 12.38.Mh, 12.38.Gc, 25.75.Dw, 25.75.Nq

I. INTRODUCTION

The anomalous suppression of the J/ψ production in heavy ion collisions [1,2] was proposed a long time ago as a possibly unambiguous signal of the onset of deconfinement [3]. In Ref. [3] it was argued that charmonium states—produced before the formation of a thermalized quark-gluon plasma (QGP)—would tend to melt in their path through the deconfined medium, since the binding (color) Coulomb potential is screened by the large number of color charges (Debye screening). This would produce an anomalous (with respect to normal nuclear absorption) drop in the J/ψ yields.[1]

Since in hadronic collisions a sizable fraction of the measured J/ψ's comes from the decay of excited charmonium states and the latter are expected to dissociate at lower temperatures, a mechanism of *sequential suppression* has been proposed, with the aim of reproducing the J/ψ suppression pattern as a function of the energy density reached in the heavy ion collision [10–14]. However, one immediately faces a few theoretical problems.

First of all, it is not even clear, at present, whether a temperature-dependent potential can describe medium modifications of quarkonia, although there are efforts aiming to derive a potential at finite temperatures from the underlying QCD (see, e.g., Refs. [15,16]). Pragmatically, one can follow a phenomenological approach, building an effective model and testing it against quarkonium properties directly calculated in QCD. On the other hand, even assuming the validity of the potential model at finite temperatures, one has to tackle the problem of finding the appropriate effective screened potential to insert into the Schrödinger equation, as it will be discussed below.

Indeed, when the mechanism of anomalous J/ψ suppression was originally proposed, the authors employed a schematic model for the $c\bar{c}$ interaction. Nowadays very precise lattice calculations of Polyakov line correlators are available, for different numbers of light dynamical fermions [17–21]. It has been known for a long time [22] that from these correlators it is possible to extract—in hot QCD, as a function of the temperature and of the $Q\bar{Q}$ separation—the change in free energy once a $Q\bar{Q}$ pair is placed in a thermal bath of gluons and light quarks.

The free energy obtained in these calculations, taken in the color-singlet channel, has been used as a temperature-dependent potential and inserted into the Schrödinger equation in a number of works [11,12,23,24]. Such a choice turned out to give very low melting temperatures for all the charmonium states: the dissociation temperatures $T_d = 1.10T_c$ [12] and $T_d = 0.99T_c$ [23] were found for the J/ψ, all the other charmonium states melting well below T_c.

On the other hand, since the free energy contains an entropy contribution, it was soon realized that employing the change in *internal* (instead of *free*) energy as an effective $Q\bar{Q}$ potential could appear better justified [25–28]. This choice results in a more attractive potential, leading to a melting temperature for the J/ψ around 1.5–$2T_c$, the other charmonium states (ψ' and χ_c) dissociating a bit above T_c. These findings appear in agreement with (quenched) lattice spectral function studies [29–33], at least for what concerns the melting temperatures of charmonia. Lattice results are starting to be available also for the bottomonium spectral function [33–35] and for the unquenched case [36]. They appear also able to explain the most recent analysis of the Na50 (Pb-Pb), Na60 (In-In) [37], and RHIC (Au-Au) [28] data on J/ψ production, which seems to favor a scenario in which only the excited states of charmonium are anomalously suppressed.

Other choices for the effective potential can be found in the literature [38–40]. In Refs. [38,39], in particular, the

[1]Potential model approaches give a *static* picture of the behavior of charmonium in the QGP, the effects of the interaction with the deconfined quarks and gluons being encoded in the *screened* $Q\bar{Q}$ interaction. Alternative pictures are available in the literature, which attempt to predict final charmonium yields in nucleus-nucleus collisions as arising from the interplay of dissociation-recombination processes [4–6] or in the framework of statistical models of hadronization [7–9].

author argues that the internal energy obtained from lattice data through the standard thermodynamical relation contains also a gluon and light quark contribution. A subtraction procedure is constructed, leading to an effective $Q\bar{Q}$ potential given by a linear combination of the lattice free and internal energies (normalized to the case with no heavy color sources), with temperature-dependent coefficients obtained from the QCD equation of state.

Results for the quarkonium dissociation temperatures, in potential models based upon lattice data, appear to be consistent with independent lattice results from spectral functions calculations. It would be, however, desirable to test it against other observables.

Actually, full information on the fate of the $Q\bar{Q}$ states in thermal equilibrium in a hot environment is encoded, depending upon the channel one is considering, in the meson spectral functions. The latter can be extracted from the Euclidean temporal correlators of mesonic currents (measured on the lattice) by inverting an integral transform. Such a task is usually achieved with a technique referred to as maximum entropy method (MEM) [41,42] and lattice results using this method can be found in Refs. [29–36]. At present, from finite temperature lattice meson spectral functions one can extract important information on the fate of the ground state in the different quantum number channels, concerning its position, strength, and melting temperature. Unfortunately, no reliable information can be extracted so far on the excited states, due to the difficulty of disentangling their peaks (if any) from lattice artifacts. Although this is not a severe limitation for charmonium studies, where one expects just a few states to (possibly) survive after the phase transition (J/ψ, χ_c, and ψ', the latter being the only excited state), this is no longer true for the bottomonium. At the ALICE experiment, for instance, one expects a sizable production of $b\bar{b}$ pairs [43]. The knowledge of the melting temperature of the different states is then important in order to develop a reliable model of sequential suppression to be eventually compared with the experimental data.

In this regard, it is clearly of importance to demonstrate that potential model calculations are consistent with the results obtained from the lattice spectral functions. Although, as we shall see, definite conclusions cannot be drawn yet, our work constitutes a promising consistency check of the potential model, given the present status of lattice calculations at finite temperatures.

Since the reliability of MEM to extract the spectral functions is not fully established yet, the check of consistency of the potential model has been mainly devoted to a direct comparison with the Euclidean correlators in a number of papers [44–49]. In these works the authors, starting from different screened potentials, calculate in a given channel the corresponding charmonium spectral function, which gets contributions both from bound states (as long as they are supported by the potential) and (starting from a threshold energy) from scattering states. Convoluting the spectral function with a thermal kernel, they eventually obtain the charmonium correlator along the imaginary temporal direction. Such a quantity can then be compared with the ones measured on the lattice. In Refs. [44–47], the authors point out that this procedure leads to a disagreement between lattice and potential model results. Hence, they conclude that a study of the $Q\bar{Q}$ states in the QGP in terms of screened potentials may not be able to catch the right physics. On the other hand, the authors of Ref. [48] propose curing the discrepancy (at least in the pseudoscalar channel) by keeping in the continuum part of the potential model spectrum only the resonant contributions, i.e. by subtracting the free gas states. We believe that this procedure might be incorrect, since the evaluated correlator has to be compared with the lattice ones, which do have a free gas (infinite temperature) limit.

The comparison between lattice data and potential model calculations is usually done by considering a quantity constructed *ad hoc*, to display the temperature dependence of quarkonium properties, namely, the ratio between Euclidean correlators above and below the critical temperature (see the next section). In a potential model this ratio turns out to be very sensitive to the treatment of the continuum, e.g. to the threshold energy. This is clearly a problem for the calculation of correlators below the critical temperature, since, for instance, at $T = 0$ the potential model is based on confining potentials and the continuum spectrum has to be added by hand. Second, lattice calculations appear to be dominated by artifacts due to the finite lattice spacing right in the continuum region, leading to unphysical peaks in the spectral functions, even in the infinite temperature limit [36,50]. Moreover, the asymptotic high energy behavior, $\sigma(\omega) \sim \omega^2$, of the continuum spectral functions is not reproduced by lattice calculations, since the finite lattice spacing provides an ultraviolet cutoff.

In this paper, following Refs. [26,38,39], we extract from the lattice data for Polyakov line correlators an effective temperature-dependent $Q\bar{Q}$ potential and we use it in order to understand to which extent a comparison with mesonic temporal correlators obtained on the lattice can be pursued. In particular, we study the effect of different models for the continuum and we try to keep under control the uncertainties introduced by the need of calculating correlators below T_c by employing the effective potential derived from lattice data for $T < T_c$ as well.

The paper is organized as follows: in Sec. II we first briefly review the formalism of finite temperature quarkonium spectral functions and imaginary time correlators and then the procedure followed to extract the effective $Q\bar{Q}$ potential from lattice data; in Sec. III we compare the outcome of the potential model to results from lattice calculations, both for the spectral functions and the Euclidean correlators; finally, in Sec. IV we summarize and discuss our results.

II. FORMALISM

A. Lattice correlators and spectral functions

The standard object introduced in lattice studies of quarkonium properties at finite temperature T is the Euclidean time correlator, defined as the thermal expectation value of a hadronic current-current correlation function in Euclidean time τ for a given mesonic channel H (see, e.g., Ref. [51], Chap. 7):

$$G_H(\tau, T) = \langle j_H(\tau) j_H^\dagger(0) \rangle, \tag{1}$$

where $j_H = \bar{q}\Gamma_H q$ and $\Gamma_H = 1,\ \gamma_5,\ \gamma_\mu,\ \gamma_\mu\gamma_5$. The four vertex operators Γ_H correspond, respectively, to the scalar, pseudoscalar, vector, and axial-vector mesonic channels, which in turn, at zero temperature, correspond to the χ_{c0} (χ_{b0}), η_c (η_b), J/Ψ (Υ), and χ_{c1} (χ_{b1}) quarkonium states for the $c\bar{c}$ ($b\bar{b}$) system, respectively. Although the correlation functions can in general be defined for any spatial momentum p, most lattice studies are restricted to the case $p = 0$ and we shall consider, in the following, only this case.

The correlators of Eq. (1) are directly evaluated in lattice QCD, whereas physical observables are related to the spectral function σ_H, i.e. to the imaginary part of the real time retarded correlators. The two quantities are connected by an integral transform

$$G_H(\tau, T) = \int_0^\infty d\omega \sigma_H(\omega, T) K(\tau, \omega, T), \tag{2}$$

which is regulated by the temperature kernel

$$K(\tau, \omega, T) = \frac{\cosh[\omega(\tau - 1/2T)]}{\sinh[\omega/2T]}, \tag{3}$$

the energy integration extending over the whole spectrum.

Extracting the continuous spectral function from the discrete and finite—and usually rather limited—set of lattice data is an ill-posed problem. It has been tackled through the application of the MEM [41,42], which appears to yield promising results, although its reliability has yet to be confirmed.

The MEM analysis has been applied by different groups to the $c\bar{c}$ system, both below and above the critical temperature and mainly in the quenched approximation (see, however, Ref. [36] for a study in the presence of dynamical fermions). The spectral functions obtained in these studies present, schematically, similar features: a well-defined peak in correspondence to the ground state meson in a channel of given angular momentum (S or P wave) up to the dissociation temperature; inability to resolve radial excitations; presence in the highest part of the spectrum of peaks that are associated to lattice artifacts. Actually, the most meaningful information extracted from the lattice spectral functions concerns the existence and mass value of the lowest quarkonium states at a given temperature.

However, the survival, e.g., of the J/Ψ up to temperatures around 1.5–$2T_c$ has important consequences for the interpretation of heavy ion experiments and it has raised the need for a confirmation not suffering from the uncertainties of the MEM analysis. A procedure has been devised that makes direct use of the Euclidean correlators, by comparing the behavior of the correlators above and below T_c [29]. Specifically, one introduces the ratio between the correlation function $G_H(\tau, T_>)$ of Eq. (2) at a temperature $T_> > T_c$ and the so-called *reconstructed correlator*

$$G_H^{\rm rec}(\tau, T_>, T_<) = \int d\omega \sigma_H(\omega, T_<) K(\tau, \omega, T_>), \tag{4}$$

calculated using the kernel at $T_> > T_c$ and the MEM spectral function at some reference temperature $T_< < T_c$. This procedure should eliminate the trivial temperature dependence due to the kernel and differences from one in the ratio should then be ascribed to the temperature dependence of the spectral function. Furthermore, the MEM result for $\sigma_H(\omega, T_<)$—because of the larger number of lattice sites at low temperature—is more robust. On the other hand, at high temperature the correlator is directly measured on the lattice, thus avoiding the extraction of the spectral function with the MEM procedure.

Indeed, lattice studies show that the ratio $G_H/G_H^{\rm rec}$ stays around one up to the same dissociation temperatures extracted from the MEM analysis and then it departs from one following different patterns in the different channels [29,33].

The other approach followed in the literature in the determination of the quarkonia dissociation temperatures—which is based on the use of effective potentials for the quarkonium systems—has reached similar conclusion about the dissociation temperatures, at least when making use of effective potentials extracted from lattice data on $Q\bar{Q}$ free energies at finite temperature [26,38,39].

In a potential model approach, one solves the Schrödinger equation for a given potential, thus getting not only the spectrum but also the wave functions of the $Q\bar{Q}$ pair. It is then fairly straightforward to get the corresponding spectral function as the imaginary part of the $Q\bar{Q}$ propagator, namely

$$\begin{aligned}\sigma_H(\omega, T) &= \frac{1}{\pi} \mathrm{Im} G_H(\omega) = \sum_n |\langle 0|j_H|n\rangle|^2 \delta(\omega - E_n) \\ &= \sum_n F_{H,n}^2 \delta(\omega - M_n) + \theta(\omega - s_0) F_{H,\omega - s_0}^2,\end{aligned} \tag{5}$$

where n represents all the relevant quantum numbers (in the second line the sum over n actually stands for both the sum over discrete states and the integration over the continuum) and $E_n = s_0 + \epsilon_n$, s_0 being the continuum threshold and ϵ_n the eigenvalue associated to the state $|n\rangle$. In the last line we have separated the discrete and continuum contributions, introducing the couplings $F_{H,n} \equiv \langle 0|j_H|n\rangle$

and $F_{H,\epsilon} \equiv \langle 0|j_H|\epsilon\rangle$ and the bound state masses M_n (a normalization of the discrete and continuum states as $\langle n|n'\rangle = \delta_{nn'}$ and $\langle \epsilon|\epsilon'\rangle = \delta(\epsilon - \epsilon')$, respectively, is understood).

Following Ref. [52] (see also Ref. [46]), one can express the couplings in terms of the wave function at the origin for the S-states (pseudoscalar and vector channels),

$$F_{PS}^2 = \frac{N_c}{2\pi}|R(0)|^2 \quad \text{and} \quad F_V^2 = \frac{3N_c}{2\pi}|R(0)|^2, \tag{6}$$

and in terms of the first derivative of the wave function at the origin for the P-states (scalar and axial-vector channels),

$$F_S^2 = \frac{9N_c}{2\pi m^2}|R'(0)|^2 \quad \text{and} \quad F_A^2 = \frac{9N_c}{\pi m^2}|R'(0)|^2, \tag{7}$$

N_c being the number of colors and m the quark mass.

By inserting the spectral function of Eq. (5) into Eq. (2), one gets the potential model expression for the Euclidean correlators:

$$G_H(\tau, T) = \sum_n F_{H,n}^2 K(\tau, M_n, T) + \int_0^\infty d\epsilon F_{H,\epsilon}^2 K(\tau, \epsilon + s_0, T). \tag{8}$$

Some care is necessary in dealing with the continuum part of the spectral function. Indeed, in Eq. (8) the integration over the excitation energy can reach pretty high values, especially for small τ's, probing regions where the nonrelativistic dispersion relation is no longer valid. Actually, the asymptotic relativistic spectral function $\sigma_H(\omega)$ that one gets in perturbative QCD is known to be proportional to ω^2 in every channel, whereas it is easy to check that the nonrelativistic solution of the Schrödinger equation in the free case goes like, e.g., $\omega^{1/2}$ for the S-states. The difference is due to the different phase space and it can be accounted for by simply renormalizing the wave function with a phase space factor [53]. In the calculations discussed below, we will be using such wave functions, renormalized to account for relativistic kinematical effects.

Note that in potential model calculations of the spectral functions, a mixed representation has been sometimes employed, with a continuum part approximated using the perturbative QCD expression with a threshold extracted from the effective potential [44,46]:

$$\sigma_H(\omega, T) = \sum_n F_{H,n}^2 \delta(\omega - M_n) + \frac{3}{8\pi^2}\omega^2 \theta(\omega - s_0) f_H(\omega, s_0), \tag{9}$$

where the function f_H is given by leading order perturbative calculations [54–56] as

$$f_H(\omega, s_0) = \left[a_H + b_H \frac{s_0^2}{\omega^2}\right]\sqrt{1 - \frac{s_0^2}{\omega^2}}. \tag{10}$$

At leading order, the coefficients (a_H, b_H) are $(1, -1)$, $(1, 0)$, $(2, 1)$, and $(2, -3)$, for the scalar, pseudoscalar, vector, and axial-vector channels, respectively. This form for the spectral function is affected by an obvious inconsistency between the bound and the continuum parts of the spectrum. Nevertheless, in the following we make use also of this expression in order to test the model dependence of our results.

B. Effective potentials from lattice data

In Ref. [26] we have provided a unified parametrization of the temperature and separation dependence of the lattice data for the color-singlet $Q\bar{Q}$ free energy F_1 in the case of quenched [17], 2-flavor [20], and 3-flavor [21] QCD.

In the following we employ the parametrization obtained there for the case $N_f = 0$—since most lattice calculations of Euclidean correlators are in quenched approximation—but we shall also consider $N_f = 2$, since in this case lattice data for the free energy are available to us also at temperatures $0.76 \leq T/T_c \leq 1$ [20], and one can use them to study the behavior of the correlation functions through the phase transition. We refer the reader to Ref. [26] for a detailed description of the fitting procedure.

Although in past work the free energy F_1 has been directly used as an input for the $Q\bar{Q}$ potential energy, more recently it has been recognized that the $Q\bar{Q}$ internal energy U_1 provides a more appropriate candidate. Since the two quantities are connected by the well-known relation

$$F = U - TS, \tag{11}$$

once a suitable parametrization of the temperature dependence for the free energy has been obtained, one can subtract the entropy contribution and get the color-singlet internal energy as

$$U_1 = -T^2 \frac{\partial(F_1/T)}{\partial T}. \tag{12}$$

The latter has been employed in Ref. [26] as the effective $Q\bar{Q}$ potential in the Schrödinger equation, getting good agreement with the charmonium dissociation temperatures extracted from lattice calculations of the spectral functions.

However, the use of the internal energy (12) is not fully satisfactory yet. From the theoretical point of view, as pointed out in Ref. [38] and thoroughly discussed in Ref. [39], the internal energy of Eq. (12) actually contains the sum of two contributions: the genuine $Q\bar{Q}$ potential energy, including the interaction of the heavy quarks with the thermal bath of gluons (and light quarks, for $N_f \neq 0$); but also a contribution due to the variation of the gluon (and light quarks, for $N_f \neq 0$) internal energy in the presence of the $Q\bar{Q}$ pair.

Also the comparison with independent lattice results presents some shortcomings. In fact, although it is quite successful in providing dissociation temperatures in agree-

ment with direct lattice estimates, its asymptotic ($r \to \infty$) value—employed to define the threshold energy entering into the continuum part of the spectral function—turns out to have a sharp temperature dependence around the critical temperature. This in turn is reflected, as we shall see in the next section, into a temperature dependence of the correlation functions which is not observed on the lattice.

In this work we follow the procedure described in Ref. [38] in order to separate the true $Q\bar{Q}$ internal energy, $U_1^{Q\bar{Q}}$, from the gluon and light quark contribution. The effective potential entering into the Schrödinger equation is defined as [F_1 and U_1 are the same quantities considered in Eq. (12)]

$$\begin{aligned} V_1(r,T) &\equiv U_1^{Q\bar{Q}}(r,T) - U_1^{Q\bar{Q}}(r\to\infty,T) \\ &= f_F(T)[F_1(r,T) - F_1(r\to\infty,T)] \\ &\quad + f_U(T)[U_1(r,T) - U_1(r\to\infty,T)], \end{aligned} \tag{13}$$

where

$$f_F(T) = \frac{3}{3 + a(T)}, \tag{14a}$$

$$f_U(T) = \frac{a(T)}{3 + a(T)} \tag{14b}$$

and

$$a(T) = \frac{p}{\epsilon/3}, \tag{15}$$

p and ϵ being the pressure and energy density of a homogeneous system of quarks and gluons, respectively. These thermodynamical quantities have been obtained in quenched [57] and 2-flavor [58] QCD as a function of temperature and we display in Fig. 1 the resulting ratio (15) in the range of temperatures we are interested in. Note that the weight functions f_F and f_U turn out to vary in the range $3/4 \lesssim f_F \lesssim 1$ and $0 \lesssim f_U \lesssim 1/4$, respectively, a fact which explains why the $Q\bar{Q}$ potential is closer (but not identical) to the free energy F_1 than to the internal energy U_1.

The asymptotic value of the $Q\bar{Q}$ internal energy, $U_1^{Q\bar{Q}}(r\to\infty,T)$, is used to define the continuum threshold, $s_0(T) = 2m + U_1^{Q\bar{Q}}(r\to\infty,T)$ and we compare it in Fig. 2 to the asymptotic value of the internal energy as obtained from Eq. (12), i.e. without subtracting the gluon and light quark contribution. The sharp variation of U_1 around T_c—which, as discussed in the next section, leads to correlation functions in contrast with lattice calculations—is evident, whereas $U_1^{Q\bar{Q}}$ displays a much smoother transition.

The effective potential based upon $U_1^{Q\bar{Q}}$ is less attractive than the one based upon U_1 (but still more attractive than the one based upon F_1), a fact which gives rise to slightly lower dissociation temperatures. Values for the latter in accord with the results from lattice spectral function studies can be obtained by using quark masses slightly higher than the values of the Particle Data Group listing [59]. For instance, in Ref. [39] dissociation temperatures compatible with the lattice phenomenology have been found using a charm quark mass of 1.4–1.5 GeV. Note that the lattice free energies employed to parametrize the effective $Q\bar{Q}$ potential have been obtained for infinitely heavy quark mass and that the lattice calculations of correlation functions use a variety of quark masses, usually chosen in order

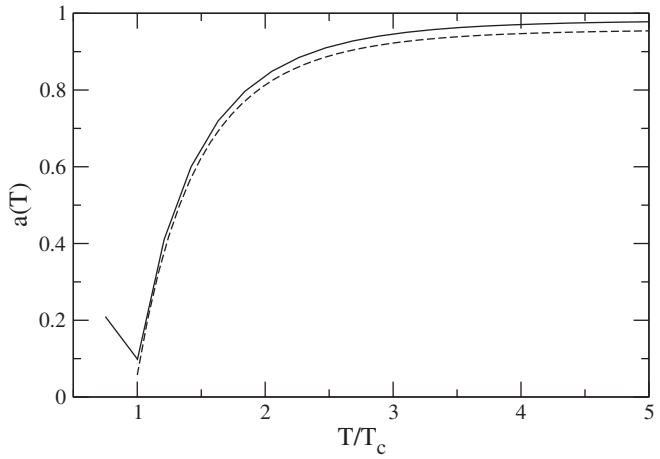

FIG. 1. The ratio $a(T) = 3p/\epsilon$ as a function of T for $N_f = 0$ [57] ($T \geq T_c$, dashed line) and $N_f = 2$ [58] ($T \geq 0.76T_c$, solid line).

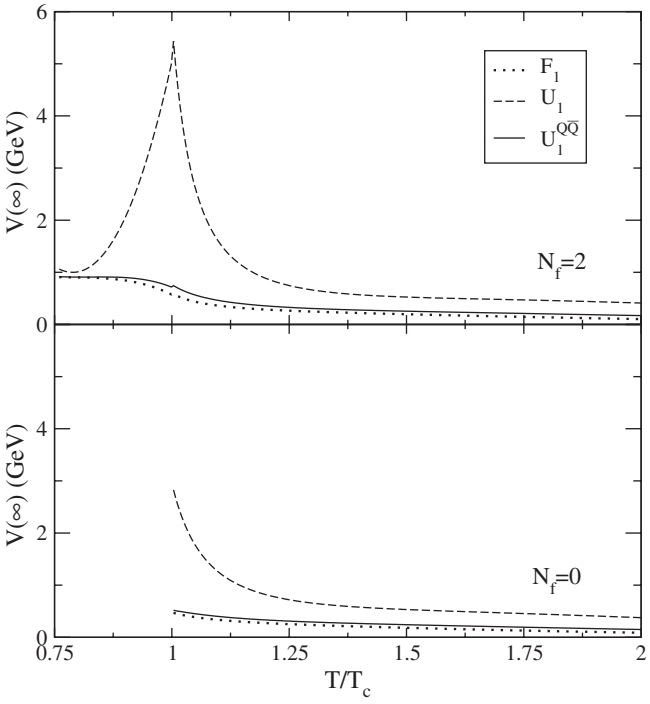

FIG. 2. The asymptotic values of the lattice free energy [20] (dotted), the total internal energy of Eq. (12) (dashed), and the $Q\bar{Q}$ internal energy $U_1^{Q\bar{Q}}$ (solid) in 2-flavor and quenched QCD.

to reproduce the mass of the charmonium (bottomonium) ground state.

Here we solve the Schrödinger equation using an effective quark mass defined as $\tilde{m}(T) = m + U_1^{Q\bar{Q}}(T)/2$, which, beside improving the binding of the $Q\bar{Q}$ pair, can be naturally interpreted as a thermal mass. Using this definition, the continuum threshold is given as $s_0(T) = 2\tilde{m}(T)$. Our choice implies that the same thermal mass is employed both in the kinetic term of the effective Hamiltonian and for the energy of the heavy quark at rest in the plasma. In principle, nothing prevents these two masses from assuming different values. While the threshold mass can be extracted from the available lattice data, in order to evaluate the thermal correction to the kinetic operator one should know the momentum dependence of the heavy quark self-energy in the QGP. Lacking the above information, here we choose to ignore such a distinction. Note that in a nonrelativistic QED plasma a moving test charge receives a positive thermal correction to its mass, which is slowly decreasing with the temperature [60]. Our choice is in qualitative agreement with this rigorous result obtained in another contest. On the other hand, it has been argued [46] that the thermal mass should not be used in the Schrödinger equation, since in the bound state the heavy quarks should not feel the effect of the medium. Yet, the quantitative differences between the two approaches are quite moderate, well below other uncertainties present in the problem.

III. RESULTS

In this section we use the effective potentials of Eq. (13) to calculate spectral and correlation functions by solving the Schrödinger equation,

$$\left[-\frac{\boldsymbol{\nabla}^2}{\tilde{m}} + V_1(r,T)\right]\psi_\varepsilon(\boldsymbol{r},T) = \varepsilon(T)\psi_\varepsilon(\boldsymbol{r},T), \qquad (16)$$

for the $Q\bar{Q}$ eigenvalues $\varepsilon(T)$ and the eigenfunctions $\psi_\varepsilon(\boldsymbol{r},T)$. The dissociation temperatures for the lowest $c\bar{c}$ and $b\bar{b}$ states are shown in Table I. Since the potential is spin independent, the two S-states, pseudoscalar, and vector (or P-states, scalar, and axial-vector) are degenerate.

With respect to the previous findings with the full internal energy [26], one now observes a reduction of the dissociation temperatures: in the $c\bar{c}$ channel the ground state melts around ≈ 1.5–$1.6T_c$, whereas the excited states already melt around the critical temperature; in the $b\bar{b}$ channel the ground state melts above $3T_c$ and the excited states around ≈ 1.1–$1.2T_c$. For comparison, in the table we also report (in square brackets) the dissociation temperatures obtained in Ref. [26] using the full internal energy, in the cases where the same quark mass had been employed (bottomonium for $m_b = 4.3$ GeV).

In Figs. 3 and 4 we show the mass, $M = 2m + U_1^{Q\bar{Q}}(r \to \infty, T) + \varepsilon(T)$, of the lowest S-wave and P-wave states, respectively, as a function of temperature. We note that in the $c\bar{c}$ channel the use of quark masses slightly larger than the values obtained from the $T = 0$ phenomenology results in meson masses heavier than $T = 0$ potential model calculations. While the latter use quark masses and effective potentials adjusted to fit the experimental data, here we employ potentials extracted from lattice data, which have been obtained from *static* (infinitely heavy) quark sources. It can then be expected that quantities directly sensitive to the input quark mass are not well reproduced. This is an intrinsic limitation of this approach, which should be much less relevant for the heavier $b\bar{b}$ system, as it could be tested as long as lattice estimates for the $b\bar{b}$ dissociation temperatures will be available.

Note, however, that the more relevant point in the comparison to the lattice spectral functions is the temperature dependence of the physical observables. From Figs. 3 and 4 one can see that, apart from a narrow range of temperatures

TABLE I. Spontaneous dissociation temperatures (in units of T_c) of the lowest $c\bar{c}$ and $b\bar{b}$ states. The values in square brackets have been taken from Ref. [26] (see text); the ones labeled with (*) have been obtained with a potential extrapolated beyond the temperature range of the lattice data ($T \lesssim 2T_c$ for $N_f = 2$).

	$N_f = 0$		$N_f = 2$	
	$m_c = 1.4$ GeV	$m_c = 1.6$ GeV	$m_c = 1.4$ GeV	$m_c = 1.6$ GeV
J/ψ, η_c	1.40	1.52	1.45	1.59
χ_c	<1	<1	1.00	1.00
ψ'	<1	<1	0.98	0.99
	$m_b = 4.3$ GeV	$m_b = 4.7$ GeV	$m_b = 4.3$ GeV	$m_b = 4.7$ GeV
Υ, η_b	2.96 [4.5]	3.18	3.9(*) [6.7(*)]	4.4(*)
χ_b	1.13 [1.55]	1.15	1.15 [1.63]	1.17
Υ'	1.12 [1.40]	1.14	1.13 [1.43]	1.15

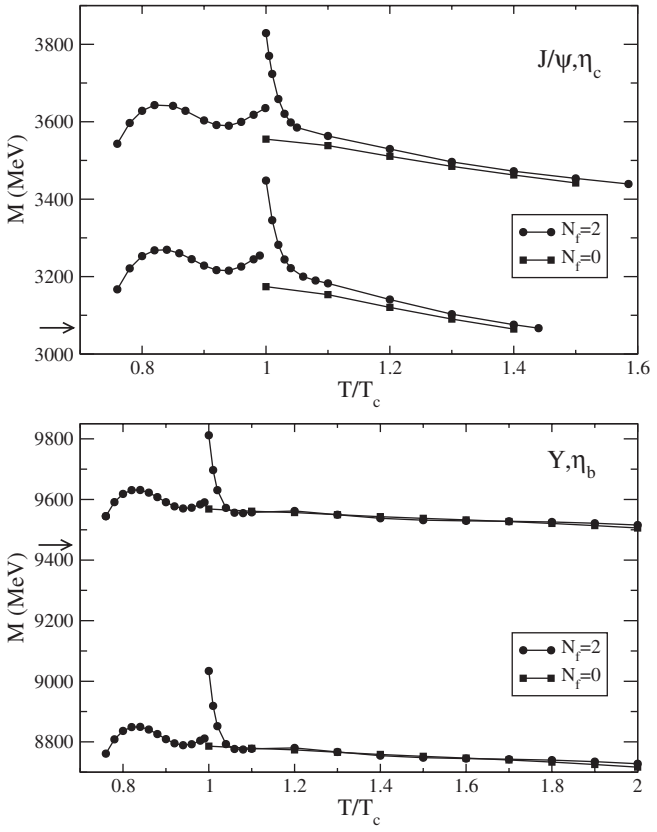

FIG. 3. Mass as a function of temperature of the lowest S-wave $c\bar{c}$ (upper panel) and $b\bar{b}$ (lower panel) states obtained from the solution of the Schrödinger equation. The upper curves are for a quark mass $m_c = 1.6$ GeV ($m_b = 4.7$ GeV), the lower ones for a quark mass $m_c = 1.4$ GeV ($m_b = 4.3$ GeV). The arrows point to the value of the mass at $T = 0$.

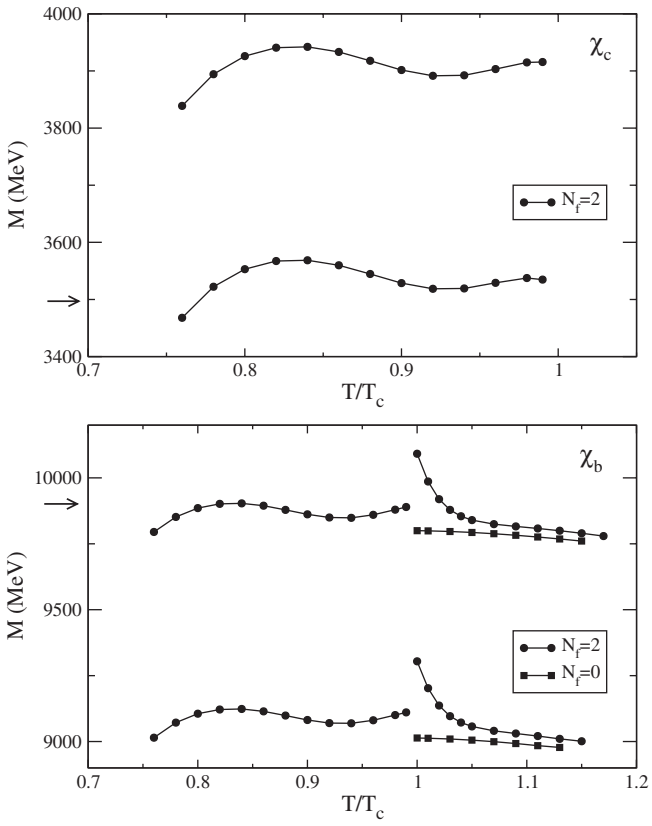

FIG. 4. As in Fig. 3, but for the lowest P-wave states.

around T_c, the variation of the masses with T is quite moderate, the difference between the maximum and minimum values being around 150–200 MeV of the S-states and ≈ 100 MeV for the P-states. This, for instance, amounts to roughly 5%–6% (2%) of the J/ψ (Υ) mass.

A slight decrease of the η_c mass in the range of temperatures explored here has also been observed in some lattice spectral studies [61]. Note that a more pronounced softening of the J/Ψ peak (here degenerate with η_c) as the temperature increases has been attributed by some authors to the presence in the vector channel of a transport contribution to the spectral function, not resolved by the MEM procedure, but nevertheless tending to move strength towards lower energies [33].

Just above T_c, one observes a slight peak in the masses for the case of 2-flavor QCD. Note that this is the range of temperatures where the T-dependence of the parameters employed to fit the lattice free energies is stronger [26], so that it might just signal the inadequacy of the parametrization at the critical temperature. It is however curious that the same behavior does not appear for $N_f = 0$, where the same parametrization has been employed.

Note that the smooth temperature dependence of the masses of the $Q\bar{Q}$ states is strictly related to the smooth T-dependence of the asymptotic $Q\bar{Q}$ internal energy, $U_1^{Q\bar{Q}}(\infty, T)$, obtained through the procedure described in Sec. II B. By employing, in the definition of the bound state mass, the total internal energy $U_1(\infty, T)$, one would get much higher (by a few GeV) masses around the critical temperature (see Fig. 2).

Other observables can be easily calculated in the potential model. As an example, we show in Fig. 5, for the $c\bar{c}$ system, the square of the S-wave radial wave function, $R(0)^2$, and the square of the first derivative of the P-wave radial wave function, $R'(0)^2$, calculated in the origin. This quantities can be related to the quarkonium decay widths for different processes (see, e.g., Ref. [51]), such as the leptonic decay rate of a neutral vector meson [63,64] or χ decay into pairs of pseudoscalar or vector mesons [65].

As one can see from the figure, the values of $R(0)$ and, particularly, of $R'(0)$ are quite stable below T_c and very close to the values at $T = 0$. Above T_c the P-wave states have melted, whereas $R(0)$ for the S-state drops almost linearly up to the dissociation temperature.

A. Spectral functions

Here we would like to compare the spectral functions calculated in the potential model to the ones extracted from

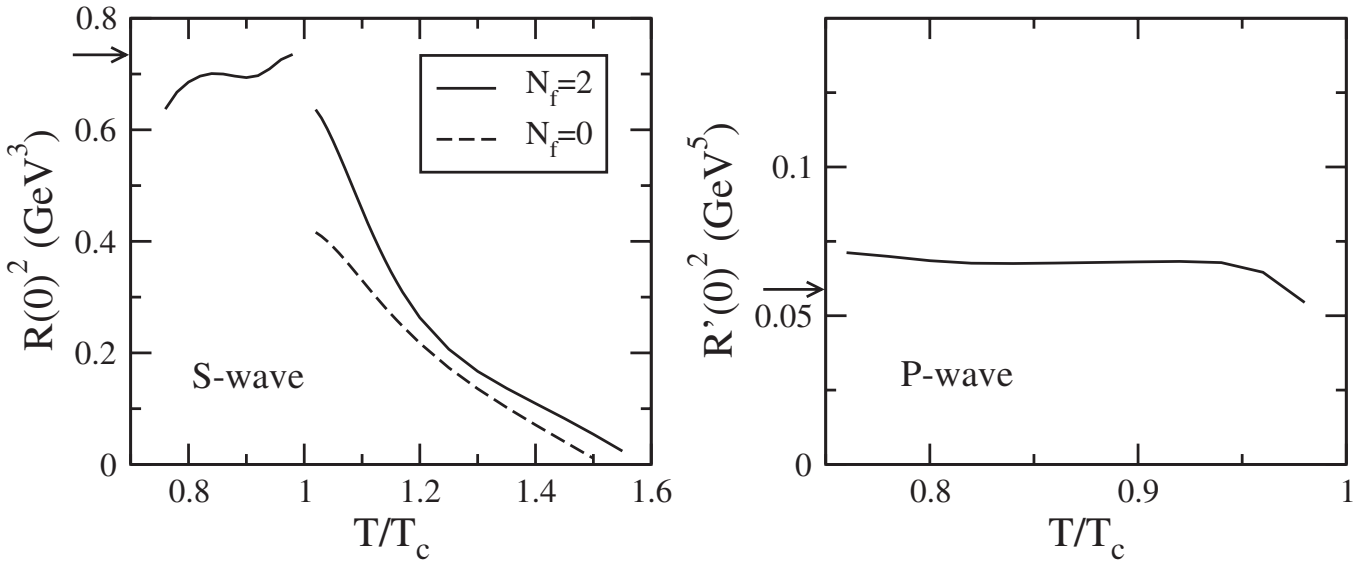

FIG. 5. Squared value in the origin, for the $c\bar{c}$ system ($m_c = 1.6$ GeV), of the S-wave radial wave function (left panel) and of the first derivative of the P-wave radial wave function (right panel), as a function of the temperature, for quenched and unquenched QCD. The arrows point to the values at $T = 0$, calculated with the Cornell potential of Ref. [62].

the lattice Euclidean correlators using MEM. To make easier a direct comparison of the spectral functions, it is convenient to modify the potential model expression of Eq. (5) in order to accommodate a width for the bound states. Indeed, the width of the bound states at finite T in the lattice spectral functions contains a contribution due to the (possible) thermal broadening of the states and a contribution due to the statistical uncertainties, the latter apparently being dominant above T_c because of the limited set of data points [33].

A width can be easily included by substituting in Eq. (5) the delta function in the bound state sector with a Lorentz distribution:

$$\sigma_H(\omega, T) = \sum_n F_{H,n}^2 \frac{1}{\pi} \frac{\Gamma_n/2}{(\omega - M_n)^2 + \Gamma_n^2/4} + \theta(\omega - s_0) F_{H,\omega - s_0}^2, \quad (17)$$

where Γ_n represents the width of the state n.

A word of caution is in order about the calculations at $T < T_c$—where we do not deal with a quark-gluon plasma, but with a still confined system. Although the use of a potential model for bound states is well assessed, at least at $T = 0$, the interpretation of the continuum spectrum is much more questionable. Here we shall use both the spectral function calculated in perturbative QCD, as usually done in the literature, and the one coming from the potential model, in order to get a feeling about the model dependence of the results. We would like however to stress that the aim of the model is to describe the physics of quarkonia at $T > T_c$ and that calculations in the confined phase are done in order to discuss the lattice results for the correlation functions, which are mainly available in the literature as ratios of functions above and below T_c (see Secs. II A and III B). In potential model calculations, the reconstructed correlators have been usually considered at zero temperature [46,48,49], adding to the bound state contribution—calculated with a phenomenological confining potential—the perturbative QCD continuum. This choice obviously poses another problem of consistency (besides the one, already mentioned, of the consistency between the bound and the continuum spectra), since above T_c one is using a lattice-derived potential and at $T = 0$ a phenomenological (fitted to the data) one. Incidentally, the phenomenological parameters of the $T = 0$ potential adopted in the above works (i.e., the coefficients of the Coulomb and linear terms) turn out to be quite different with respect to the ones employed in normalizing the free energies at short distances [20]. The use, also below T_c, of lattice-derived potentials should give one a feeling about these model dependencies.

In Fig. 6 we display the $c\bar{c}$ spectral function for the S-states for quenched and unquenched QCD, both below and above T_c (since we neglect the hyperfine spin-spin interaction the J/ψ and η_c states are degenerate and the corresponding spectral functions differ for trivial factors). In the left-hand panels, we employ—for the continuum part of the spectral function—the solution of the Schrödinger equation [Eq. (17), see the discussion in Sec. II A], whereas in the right-hand panels we employ the perturbative expression [see Eq. (9)]. In all cases a width $\Gamma_n = 100$ MeV has been used for the discrete states. Here and in the following calculations, we employ $m_c = 1.6$ GeV and $m_b = 4.7$ GeV for the quark mass.

In this figure, one can note a marked peak of constant strength and almost fixed position below T_c, corresponding

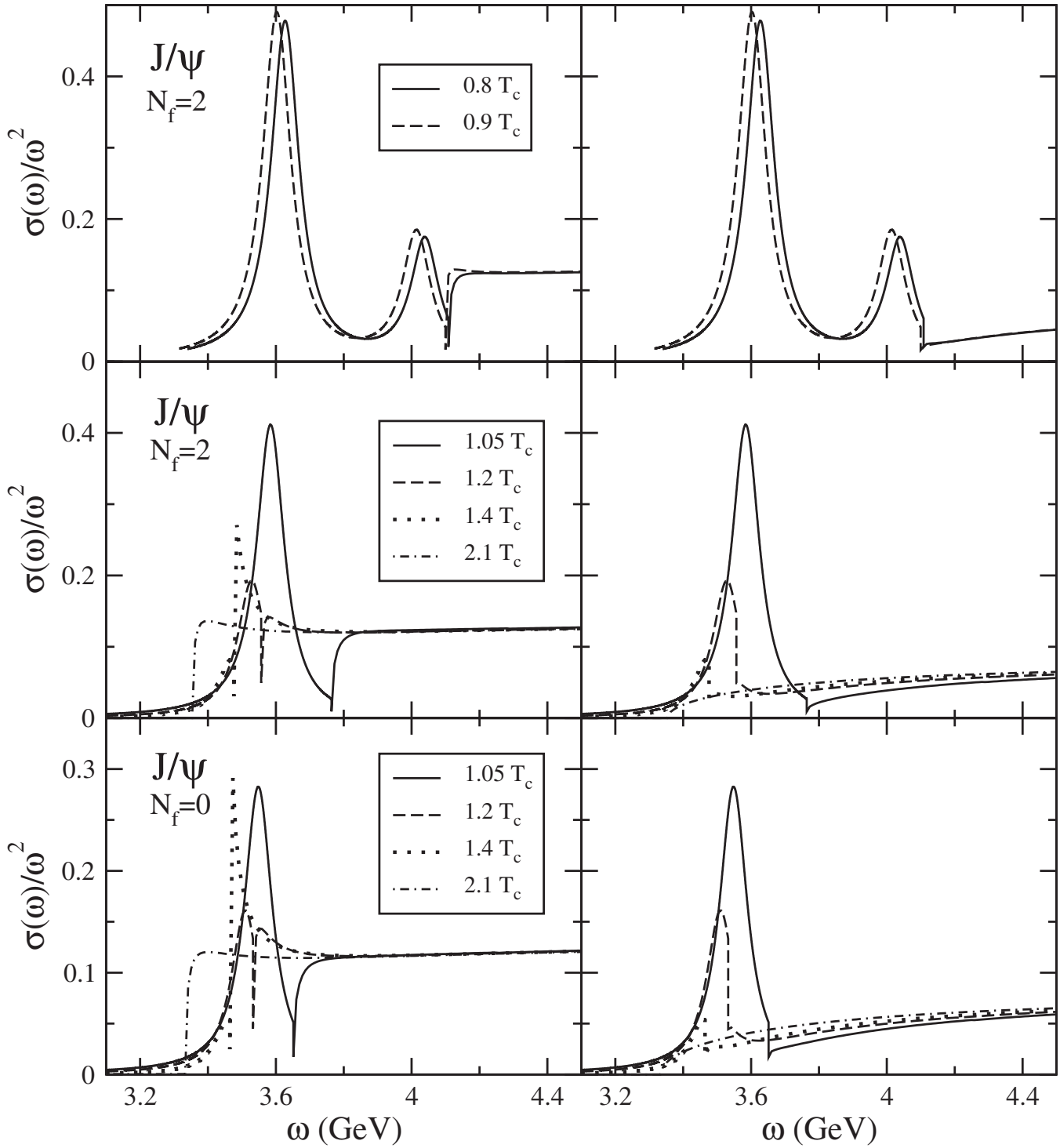

FIG. 6. The J/ψ spectral function divided by ω^2 as a function of ω for $N_f = 2$ and $N_f = 0$ at several temperatures below and above T_c; in the left panels the continuum part of the spectrum comes from the solution of the Schrödinger equation, in the right panels from the perturbative expression.

to the J/ψ state, and a second smaller peak, corresponding to its first radial excitation. Above T_c only the ground state peak survives and its position moderately moves (consistently with the mild mass shift displayed in Fig. 3), whereas its strength is gradually decreasing as one approaches the dissociation temperature. There is no significant difference between $N_f = 0$ and $N_f = 2$.

Above T_c the bound state peak is clearly visible especially in the right-hand panels, where the perturbative continuum spectral function has been employed. The con-

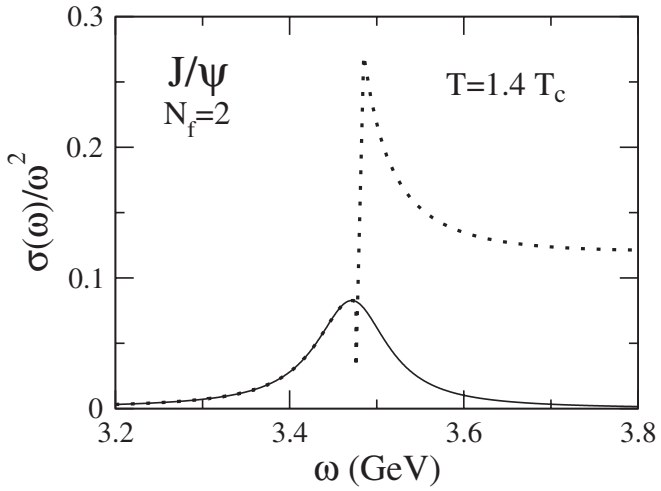

FIG. 7. The J/ψ spectral function divided by ω^2 as a function of ω for $N_f = 2$ and $T = 1.4T_c$ (dotted line). The bound state contribution (solid line) is also shown separately.

tinuum contribution calculated from the Schrödinger equation, on the other hand, shows a resonant part when the bound state energy is approaching zero and this resonant contribution tends to dominate over the bound state peak (see Fig. 7, where, as an example, the spectral function at $T = 1.4T_c$ is magnified around the threshold energy, separating the bound state and continuum contributions).

In order to show more clearly the evolution of the bound state above T_c—and to make easier a comparison with the lattice results—we display in Fig. 8 only the bound state part of the S-wave spectral function using a larger effective width, comparable to the one of the lattice charmonium spectral functions calculated in Refs. [29,33] ($N_f = 0$) and [36] ($N_f = 2$). As one can see the pattern as a function of the temperature for the position of the bound state appears to be similar to the lattice results.

The temperature dependence of the strength of the peak, instead, seems to differ from the lattice outcome. In Refs. [29,33], the S-wave spectral functions have also been extracted at various temperatures using the same number of data points, in order to compare results affected by the same statistical uncertainties: at least for the pseudoscalar state (the vector channel being more uncertain) it has been found that the spectral function maintains its strength up to $1.5T_c$. This result is, of course, affected by large errors and also depends upon the reliability of the MEM procedure. On the other hand, the potential model calculation yields a practically constant strength up to T_c and then a practically linear decrease, as it could be inferred also from Fig. 5.

In Fig. 9 we show the spectral function for the P-states in the case of unquenched QCD, using, for illustration, a width of 100 MeV (again, we neglect hyperfine splitting of scalar and axial-vector states). The continuum contribution in the left panel comes from solving the Schrödinger equation, in the right panel from the perturbative calculation. Also in this channel one can note, below T_c, a marked peak of constant strength and approximately fixed position, corresponding to the χ_c state. No bound states are present above T_c: the peak appearing in the left panel at $T = 1.05T_c$ is actually a resonance in the continuum contribution. Also the narrow peaks visible at higher energy for $T < T_c$ are embedded in the continuum. The situation of the P-wave lattice spectral functions is less clear, since this channel is much harder to study on the lattice. All the studies [29,33,36] of the $c\bar{c}$ system observe a strong modification of the spectral functions above T_c and this is usually interpreted as a signature of dissociation of the P-wave states. However, above T_c some strength is ob-

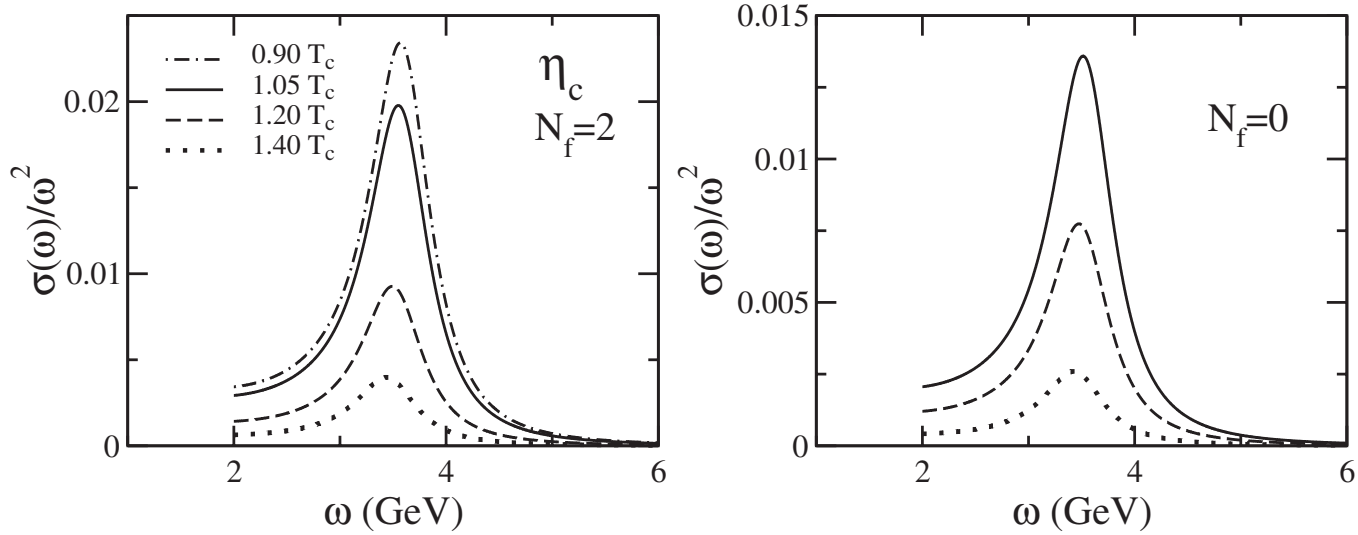

FIG. 8. Bound state contribution to the pseudoscalar spectral function divided by ω^2 for $N_f = 2$ and $N_f = 0$ at various temperatures. A width $\Gamma_n = 700$ MeV has been used.

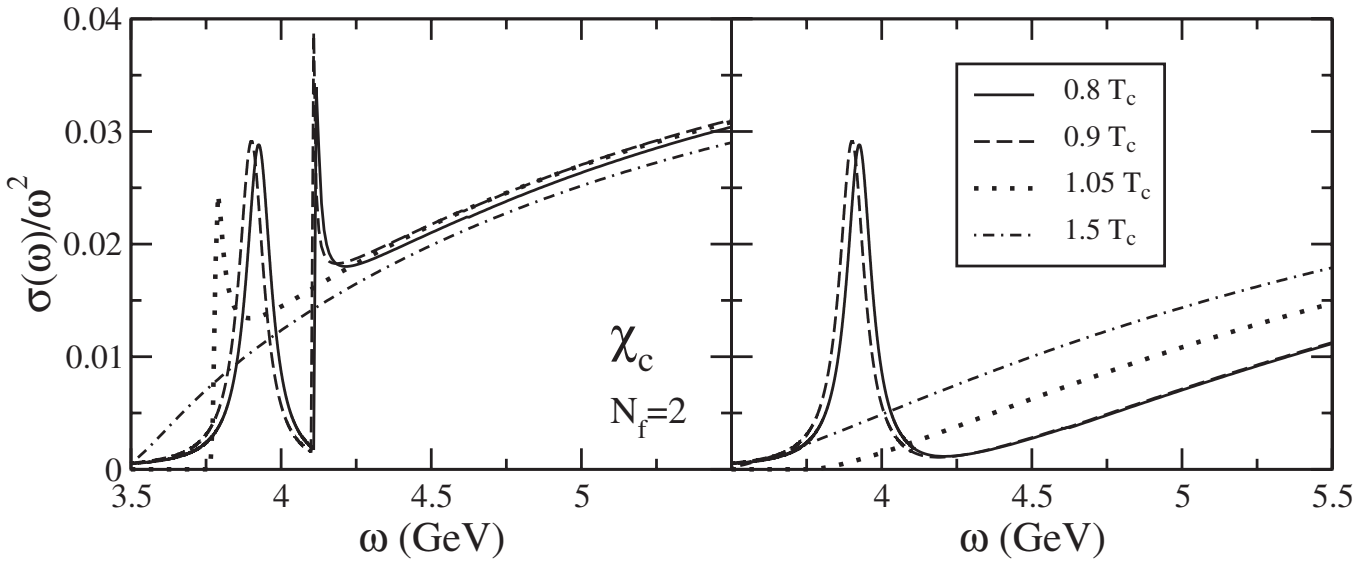

FIG. 9. The χ_c spectral function divided by ω^2 as a function of ω for $N_f = 2$ at several temperatures below and above T_c; in the left panel the continuum part of the spectrum comes from the solution of the Schrödinger equation, in the right panel from the perturbative expression.

served at very low energies, especially in the scalar channel, well below the expected continuum threshold and there is no physical explanation for these findings.

Finally, in Fig. 10 we display the bound state part of the S- and P-wave spectral functions for $b\bar{b}$ states, in the range of temperatures studied in Refs. [34,35]. The Υ state appears to be stable both in position and strength over the whole range of temperatures, whereas the χ_b state gets strongly modified approaching the dissociation temperature (see Table I). The stability in the position of the Υ and the dissociation of the χ_b at a temperature $T \cong 1.1$–$1.2T_c$ is in accord with the results from lattice calculations; the latter, however, are still preliminary and one cannot draw from them any conclusion about the evolution of the strength with T. We do not show the continuum part of the spectrum, since it is very similar to the charmonium case.

To summarize our findings for the $Q\bar{Q}$ spectral functions, we can state that the bound state part of the potential model spectrum appears to be consistent with the lattice results as far as the evolution with T of the position of the $c\bar{c}$ and $b\bar{b}$ states is concerned. On the other hand, both the evolution of the bound state strength and the shape of the continuum contribution—either perturbative or calculated in the potential model—show major differences from the lattice outcome.

B. Correlation functions

As we have already mentioned above, the reliability of the MEM procedure is still under discussion. In order to reveal the temperature dependence of the spectral function, it has been proposed to consider the ratio between the Euclidean correlator at a given temperature and the reconstructed correlator, which contains the spectral function at a reference temperature (see Sec. II A).

In lattice calculations, this has been done using as a reference temperature both some finite $T < T_c$ [29] and $T = 0$ [33]. In potential model calculations, the spectral function at $T = 0$—modeled as in Eq. (9) by using a phenomenological potential for the bound states and the perturbative QCD contribution for the continuum states—has been employed so far as a reference [46,49]. However, such a spectral function is not only affected by the inconsistency between the bound and the continuum states, but it also strongly depends upon the threshold energy s_0, which has to be treated as a parameter. Moreover, employing, for the continuum contribution in the confined phase, the perturbative QCD spectral function is at least problematic. Here we try to remove the first two sources of uncertainties by employing the spectral functions calculated from the lattice-generated potential at $T < T_c$. Of course, the problem of interpretation of the continuum spectrum is still there, but, as we shall see below, it is probably inessential.

In Fig. 11 we display the ratio G_H/G_H^{rec} for the pseudoscalar and scalar charmonium states at different temperatures, using the reconstructed correlator at $T = 0.75T_c$. Both the continuum spectra generated by solving the Schrödinger equation (left panels) and by using the perturbative expressions (right panels) are employed.

Let us first analyze the ratio at $T < T_c$. Here it turns out to be always very close to 1, not only for the case shown in the figure, but over the whole range of temperatures available to us ($0.75 < T/T_c < 1$). It strongly resembles the ratio of the correlators measured on the lattice [29]: even

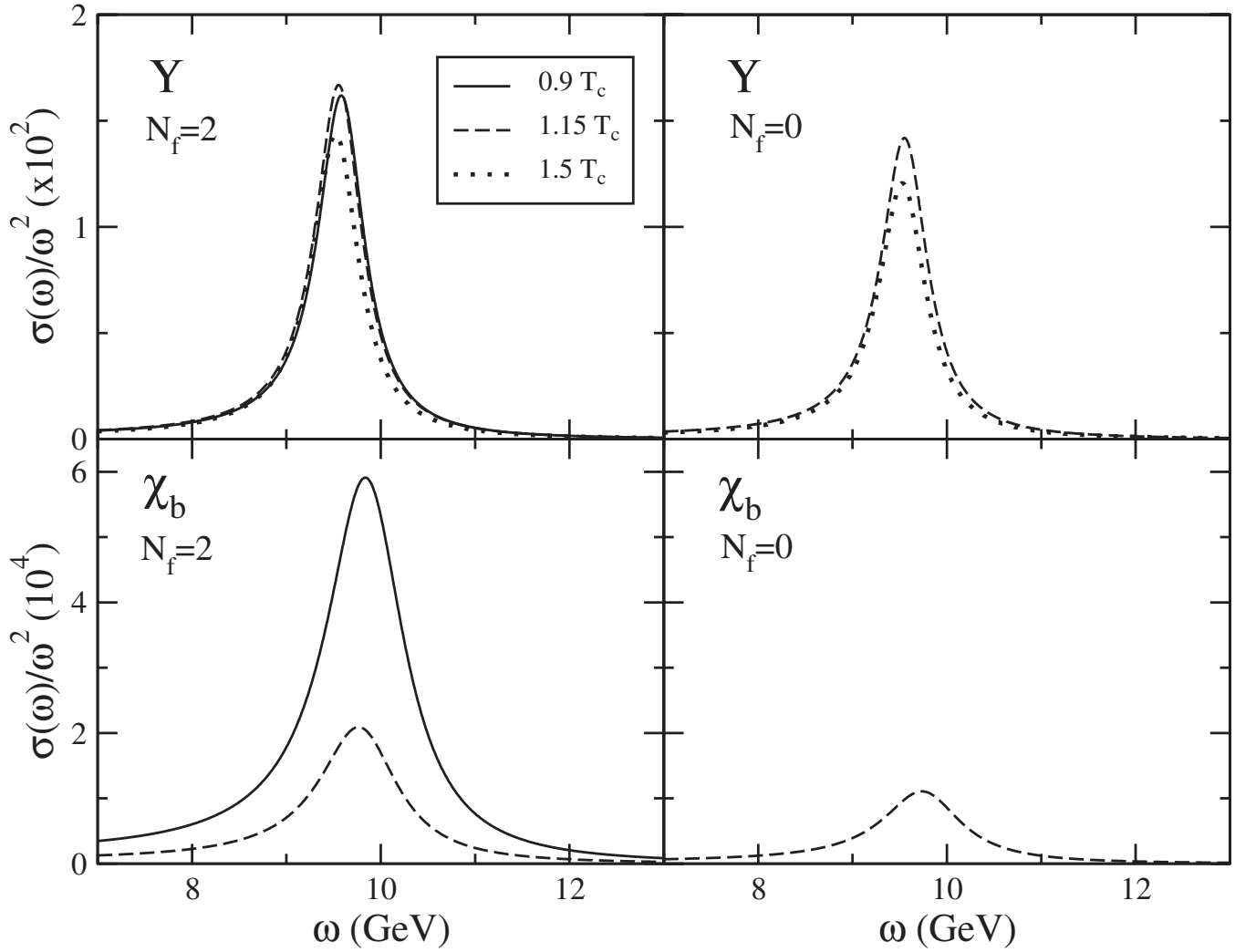

FIG. 10. Bound state contribution to the spectral function divided by ω^2 for $b\bar{b}$ states at temperatures below and above T_c. $N_f = 2$ in the left panels and $N_f = 0$ in the right panels. The widths are 650 MeV (Υ) and 1 GeV (χ_b) [34,35].

the small decrease at large τ's in the scalar channel seems to be correctly reproduced. Note that this outcome simply reflects the temperature independence of the spectral functions below T_c, as it was apparent in Fig. 6. This evolution with the temperature in our model stems from the mild dependence upon T of both the effective potential and the threshold energy, which, in turn, is due to the procedure of subtraction of the gluon and light quark contributions from the $Q\bar{Q}$ internal energy (see Sec. II B). The same quantities calculated using directly the internal $Q\bar{Q}$ energy as the effective potential would yield a strong T dependence already below T_c (see, e.g., Fig. 2).

Above T_c, the ratio in the pseudoscalar channel looks qualitatively similar to the one measured on the lattice [29,33]—at variance with the result of Refs. [46,49]—but there are important differences. In the lattice results, the ratio remains close to 1 up to the dissociation temperature and then it gradually decreases; here, the departure from one occurs as soon as the temperature grows beyond T_c and reflects the rapid change in the threshold energy visible in Fig. 2. After that, the smooth change in the threshold energy and the reduction of the bound state strength as T increases give rise to the moderate decrease of G_H/G_H^{rec} observed in Fig. 11.

In the scalar channel the situation is rather different: the ratio calculated using the perturbative continuum grows above one and then drops down, whereas in the case of the potential model continuum it is always lower than one. Both results are at variance with the lattice ones, where the ratio is uniformly growing with τ. The reason for the different behavior employing either the perturbative or the ''interacting'' continuum can be reconducted to the presence, in the latter case, of a strong resonance just above the threshold at $T < T_c$ (see Fig. 9).

As one can see, differences in the outcome from the different models employed here and in other works [46,49]

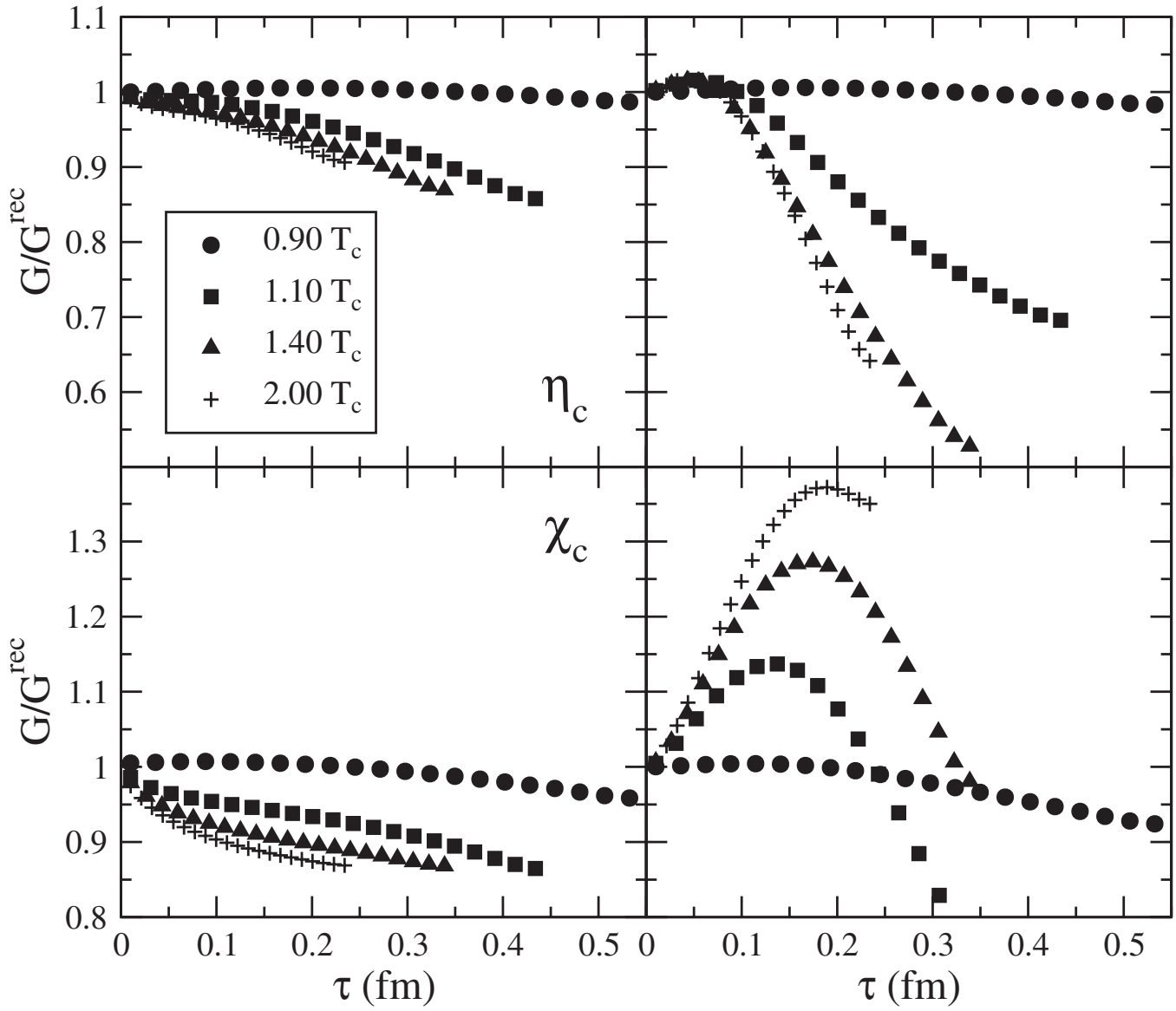

FIG. 11. Ratio G_H/G_H^{rec} for the pseudoscalar (upper panels) and scalar (lower panels) charmonium states ($N_f = 2$) at different temperatures, using the reconstructed correlator at $T = 0.75T_c$, as a function of the Euclidean time τ. In the left panels the continuum part of the spectrum comes from the solution of the Schrödinger equation, in the right panels from the perturbative expression.

can in general be understood in terms of differences in the treatment of the continuum contribution to the spectral functions (its form and/or the threshold energy). Hence, the ratio G_H/G_H^{rec} appears to be a sensitive observable in discriminating among different models. However, so far no model calculation has been able to reproduce the lattice results for every channel.

In order to understand the reason for this discrepancy, we display in Fig. 12 the spectral functions (divided by ω^2) in the pseudoscalar and scalar channels at a fixed temperature. In the same plots we also show (dot-dashed lines) the factors $\omega^2 K(\tau, \omega, T)$ by which the spectral function $\sigma_H(\omega, T)/\omega^2$ should be multiplied in order to get the integrand yielding the Euclidean correlator of Eq. (2). The factors $\omega^2 K(\tau, \omega, T)$ are shown for two values of τ, namely, a small one—where the ratio G_H/G_H^{rec} goes to one both in lattice measurements and in model calculations—and a large one—where the effects of temperature on the ratio are stronger.

As one can see from the figure, at small τ's the weighting factor $\omega^2 K$ is a rather smooth function covering a wide range of energies and the corresponding correlator gives, roughly speaking, a measure of the total strength associated to the spectral function. On the other hand, for large values of τ the weighting factor $\omega^2 K$ is a rapidly dropping function of the energy, selecting only the low energy part of the spectral function (this is, of course, a nice feature for discriminating among different models).

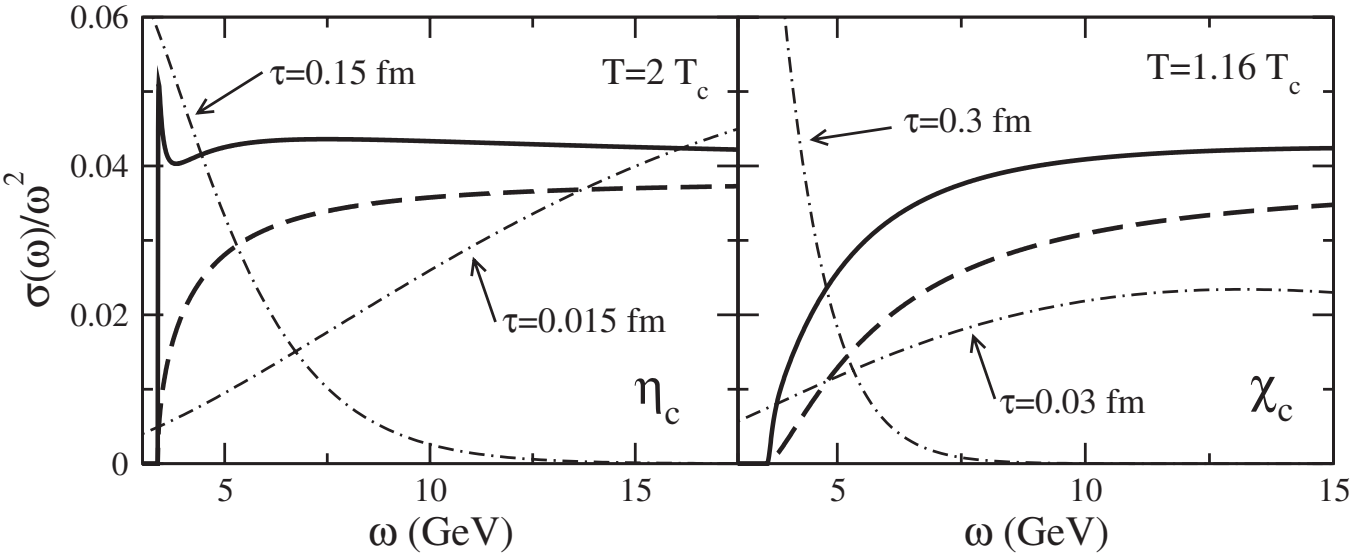

FIG. 12. Spectral functions (divided by ω^2) for $N_f = 0$ in the pseudoscalar ($T = 2T_c$) and scalar ($T = 1.16T_c$) channels as a function of the energy; both the potential model (solid line) and the perturbative QCD (dashed line) results are displayed. The dot-dashed lines represent the factor $\omega^2 K(\tau, \omega, T)$ (in arbitrary units) for two values of τ.

The discrepancy with the lattice results can be understood by comparing, e.g., Fig. 12 with Fig. 17 (pseudoscalar case) and Fig. 19 (scalar case) of Ref. [33]. In the pseudoscalar case, at $T = 2T_c$ no bound state is present in our potential model calculation. The lattice estimates at this temperature show a strong dependence upon the default model used to extract the spectral function, yielding either a significant change with respect to $T = 0$ (see Fig. 17 of Ref. [33]) or almost no temperature dependence. In any case, the small reduction ($\approx 5\%$) observed in the ratio of correlators is due to (moderate) differences between the $T = 0$ and $T = 2T_c$ spectral functions at energies $\lesssim 10$ GeV, which are dominated by the lowest energy peak visible in Fig. 17 of Ref. [33]. Our potential model calculation (solid line in Fig. 12) also presents a peak (a resonance in the continuum spectrum)—at variance with the perturbative QCD spectrum (dashed line)—and this explains the similar behavior of G_H/G_H^{rec} in our calculation and on the lattice.

In the scalar case, on the other hand, there are no resonances in the potential model calculation and no strength is present at low energy ($\lesssim 4$ GeV)—whereas some strength appears at low energy in the lattice result (Fig. 19 of Ref. [33])—and this explains the different behavior of G_H/G_H^{rec} for this channel in our calculation and on the lattice.

We would like to stress that this explanation for the discrepancy between potential model and lattice correlators does not rely upon the MEM-based lattice spectral functions, which have been used only to illustrate our argument. For instance, the exact lattice spectral function in the scalar channel at $T = 1.16T_c$ may not have the form of the MEM-based ones, but it must have, in the low energy region, more strength than the $T = 0$ spectral function in order to yield a correlator twice as large as the reconstructed one (Fig. 11 of Ref. [33]).

This analysis—together with the direct comparison of the lattice and potential model spectral functions done in the previous section—shows that the discrepancies between the two approaches are mostly located in the continuum part of the $Q\bar{Q}$ spectrum. Indeed, in this energy domain, the lattice spectral functions (which provide useful information on the properties of the ground state) suffer strong limitations, due to the inability of resolving excited/resonant states, the presence of unphysical peaks related to lattice artifacts, and the bad asymptotic high energy behavior. Note, in particular, that the presence of unphysical peaks is not related to the MEM procedure, since they appear also in the infinite temperature limit [50]. Hence, the ratio G_H/G_H^{rec} may not be a good candidate to check the consistency of the two approaches (potential models vs lattice studies).

IV. SUMMARY AND CONCLUSIONS

We have given a comprehensive treatment of quarkonia at finite temperature, within the framework of a potential model. We have constructed an effective $Q\bar{Q}$ potential as a linear combination of the finite temperature $Q\bar{Q}$ internal and free energies—in order to separate the genuine $Q\bar{Q}$ energy from the gluon and light quark contributions—and we have used as input the $Q\bar{Q}$ free energies obtained on the lattice from Polyakov loop correlators.

The effective potential that we have obtained yields dissociation temperatures for the $c\bar{c}$ and $b\bar{b}$ systems that are in agreement with estimates based on independent lattice studies of Euclidean correlators and spectral func-

tions. Specifically, we have found that in the charmonium system only the ground S-wave states (J/ψ and η_c) survive up to ≈ 1.5–$1.6T_c$, all the other states melting around the critical temperature or below; in the bottomonium system, again only the ground S-wave states (Υ and η_b) survive up to temperatures $\gtrsim 3T_c$, while χ_b and Υ' melt around ≈ 1.1–$1.2T_c$.

In order to gain deeper insight into the comparison of results based upon the potential model and lattice studies, we have also calculated the $c\bar{c}$ and $b\bar{b}$ spectral functions over a wide range of temperatures. To test the model dependence of the results, two models for the continuum spectrum have been employed: one using the interacting solution of the Schrödinger equation and one using the perturbative QCD spectrum. The evolution with the temperature of the mass of the bound states has been found in good agreement with the lattice results, while the T-dependence of the strength of the bound states agrees only below T_c. Above T_c the lattice-based spectral functions show little temperature dependence of the bound state strength, whereas in the potential model—where the strength is proportional to the coupling F_H^2—the latter drops almost linearly. On the other hand, the continuum spectrum in the two approaches shows no resemblance at any temperature.

We have also calculated in the potential model the $Q\bar{Q}$ Euclidean correlators, since these quantities are directly measured on the lattice and are not affected by the uncertainties inherent to the procedure of extraction of the lattice spectral functions. We have found good agreement with the lattice results in the pseudoscalar channel and not in the scalar one: we have shown that the agreement or disagreement between potential model and lattice in the correlators is not driven by the bound state contributions, but by the continuum spectrum. Since the latter is known to be strongly affected by artifacts due to the finite size of the lattice, the ratio of Euclidean correlators, G_H/G_H^{rec}, does not appear to be appropriate for a test of potential models vs lattice calculations.

At the present stage, the only substantial conflict between potential model and lattice predictions for quarkonium properties at finite temperature seems to be in the T-dependence of the bound state strength from the critical temperature up to the melting point, i.e. a progressive drop in the potential model and—presumably, since lattice results are available only for a few temperatures—a rapid change at the dissociation point in the spectral studies on the lattice. Lattice results for the $Q\bar{Q}$ spectral functions above T_c, however, are still affected by uncertainties related to the MEM procedure and by large statistical errors and new measurements with better statistics will probably put this outcome on firmer grounds. On the other side, one has to gain deeper insight into the connection of the potential model with the underlying QCD at finite temperature, not only to provide a solid and rigorous basis for the model, but also in order to extend its applicability (e.g., by including an imaginary part to describe the thermal broadening of the quarkonium states).

ACKNOWLEDGMENTS

A. B. would like to thank the Della Riccia foundation for financial support.

[1] M. C. Abreu *et al.*, Phys. Lett. B **477**, 28 (2000).
[2] B. Alessandro *et al.* (Na50 Collaboration), Eur. Phys. J. C **39**, 335 (2005).
[3] T. Matsui and H. Satz, Phys. Lett. B **178**, 416 (1986).
[4] L. Grandchamp and R. Rapp, Phys. Lett. B **523**, 60 (2001).
[5] L. Grandchamp and R. Rapp, Nucl. Phys. **A709**, 415 (2002).
[6] L. Grandchamp, R. Rapp, and G. E. Brown, Phys. Rev. Lett. **92**, 212301 (2004).
[7] M. Gazdzicki and M. I. Gorenstein, Phys. Rev. Lett. **83**, 4009 (1999).
[8] P. Braun-Munzinger and J. Stachel, Phys. Lett. B **490**, 196 (2000).
[9] A. Andronic, P. Braun-Munzinger, K. Redlich, and J. Stachel, nucl-th/0611023.
[10] S. Gupta and H. Satz, Phys. Lett. B **283**, 439 (1992).
[11] S. Digal, P. Petreczky, and H. Satz, Phys. Lett. B **514**, 57 (2001).
[12] S. Digal, P. Petreczky, and H. Satz, Phys. Rev. D **64**, 094015 (2001).
[13] F. Karsch, Eur. Phys. J. C **43**, 35 (2005).
[14] D. Kharzeev, C. Lourenco, M. Nardi, and H. Satz, Z. Phys. C **74**, 307 (1997).
[15] Yu. A. Simonov, Phys. Lett. B **619**, 293 (2005).
[16] M. Laine, O. Philipsen, P. Romatschke, and M. Tassler, J. High Energy Phys. 03 (2007) 054.
[17] O. Kaczmarek, F. Karsch, P. Petreczky, and F. Zantow, Phys. Lett. B **543**, 41 (2002).
[18] O. Kaczmarek, F. Karsch, P. Petreczky, and F. Zantow, Nucl. Phys. B, Proc. Suppl. **129**, 560 (2004).
[19] O. Kaczmarek, S. Ejiri, F. Karsch, E. Laermann, and F. Zantow, Prog. Theor. Phys. Suppl. **153**, 287 (2004).
[20] O. Kaczmarek and F. Zantow, Phys. Rev. D **71**, 114510 (2005).
[21] P. Petreczky and K. Petrov, Phys. Rev. D **70**, 054503 (2004).
[22] L. D. McLerran and B. Svetitsky, Phys. Rev. D **24**, 450 (1981).
[23] C. Y. Wong, Phys. Rev. C **65**, 034902 (2002).
[24] C. Y. Wong, J. Phys. G **28**, 2349 (2002).

[25] E. V. Shuryak and I. Zahed, Phys. Rev. D **70**, 054507 (2004).
[26] W. M. Alberico, A. Beraudo, A. De Pace, and A. Molinari, Phys. Rev. D **72**, 114011 (2005).
[27] H. Satz, hep-ph/0602245.
[28] H. Satz, J. Phys. G **32**, R25 (2006).
[29] S. Datta, F. Karsch, P. Petreczky, and I. Wetzorke, Phys. Rev. D **69**, 094507 (2004).
[30] M. Asakawa, T. Hatsuda, and Y. Nakahara, Nucl. Phys. **A715**, 863 (2003).
[31] M. Asakawa and T. Hatsuda, Phys. Rev. Lett. **92**, 012001 (2004).
[32] T. Umeda, K. Nomura, and H. Matsufuru, Eur. Phys. J. C **39**, 9 (2005).
[33] A. Jakovac, P. Petreczky, K. Petrov, and A. Velytsky, Phys. Rev. D **75**, 014506 (2007).
[34] K. Petrov, A. Jakovac, P. Petreczky, and A. Velytsky, Proc. Sci., LAT2005 (2005) 153.
[35] S. Datta, A. Jakovac, F. Karsch, and P. Petreczky, AIP Conf. Proc. **842**, 35 (2006).
[36] G. Aarts, C. R. Allton, R. Morrin, A. P. Ó Cais, M. B. Oktay, M. J. Peardon, and J. I. Skullerud, Proc. Sci. LAT2006 (2006) 126.
[37] C. Lourenco *et al.* (Na60 Collaboration), Proc. Sci., HEP2005 (2006) 133.
[38] C. Y. Wong, Phys. Rev. C **72**, 034906 (2005).
[39] C. Y. Wong, hep-ph/0606200.
[40] A. Di Giacomo, E. Meggiolaro, Yu. A. Simonov, and A. I. Veselov, hep-ph/0512125.
[41] M. Asakawa, T. Hatsuda, and Y. Nakahara, Prog. Part. Nucl. Phys. **46**, 459 (2001).
[42] Y. Nakahara, M. Asakawa, and T. Hatsuda, Phys. Rev. D **60**, 091503(R) (1999).
[43] B. Alessandro *et al.* (ALICE Collaboration), J. Phys. G **32**, 1295 (2006).
[44] A. Mocsy and P. Petreczky, Eur. Phys. J. C **43**, 77 (2005).
[45] A. Mocsy, Nucl. Phys. **A774**, 885 (2006).
[46] A. Mocsy and P. Petreczky, Phys. Rev. D **73**, 074007 (2006).
[47] A. Mocsy, hep-ph/0606124.
[48] C. Y. Wong and H. W. Crater, Phys. Rev. D **75**, 034505 (2007).
[49] D. Cabrera and R. Rapp, hep-ph/0611134.
[50] F. Karsch, E. Laermann, S. Stickan, and P. Petreczky, Phys. Rev. D **68**, 014504 (2003).
[51] N. Brambilla *et al.*, CERN Yellow Report, CERN-2005-005, 2005.
[52] G. T. Bodwin, E. Braaten, and G. P. Lepage, Phys. Rev. D **51**, 1125 (1995).
[53] B. Durand and L. Durand, Phys. Rev. D **25**, 2312 (1982).
[54] F. Karsch, M. G. Mustafa, and M. H. Thoma, Phys. Lett. B **497**, 249 (2001).
[55] W. M. Alberico, A. Beraudo, and A. Molinari, Nucl. Phys. **A750**, 359 (2005).
[56] G. Aarts and J. M. Martínez Resco, Nucl. Phys. **B726**, 93 (2005).
[57] G. Boyd, J. Engels, F. Karsch, E. Laermann, C. Legeland, M. Lutgemeier, and B. Petersson, Nucl. Phys. **B469**, 419 (1996).
[58] F. Karsch, E. Laermann, and A. Peikert, Phys. Lett. B **478**, 447 (2000).
[59] S. Eidelman *et al.* (Particle Data Group), Phys. Lett. B **592**, 1 (2004).
[60] S. Ichimaru, *Basic Principles of Plasma Physics—A Statistical Approach* (Addison-Wesley/W. A. Benjamin, Reading, 1973).
[61] H. Iida, T. Doi, N. Ishii, H. Suganuma, and K. Tsumura, Phys. Rev. D **74**, 074502 (2006).
[62] L. P. Fulcher, Phys. Rev. D **50**, 447 (1994).
[63] R. Van Royen and V. F. Weisskopf, Nuovo Cimento A **50**, 617 (1967); **51**, 583 (1967).
[64] R. Barbieri, Z. Kunszt, and R. Gatto, Nucl. Phys. **B105**, 125 (1976).
[65] A. Duncan and A. H. Mueller, Phys. Lett. **93B**, 119 (1980).